Studies on the double-β decay nucleus ^{64}Zn using the (d,^{2}He) reaction

E.-W. Grewe,[1] C. Bäumer,[1,*] H. Dohmann,[1] D. Frekers,[1] M. N. Harakeh,[2] S. Hollstein,[1] H. Johansson,[3] K. Langanke,[3,4] G. Martínez-Pinedo,[3] F. Nowacki,[5] I. Petermann,[3] L. Popescu,[6,†] S. Rakers,[1,‡] D. Savran,[2,4] K. Sieja,[3] H. Simon,[3] J. H. Thies,[1] A. M. van den Berg,[2] H. J. Wörtche,[2] and A. Zilges[4]

[1]*Institut für Kernphysik, Westfälische Wilhelms-Universität Münster, Germany*
[2]*Kernfysisch Versneller Instituut, University of Groningen, NL-9747 AA Groningen, The Netherlands*
[3]*Gesellschaft für Schwerionenforschung, D-64291 Darmstadt, Germany*
[4]*Institut für Kernphysik, Technische Universität Darmstadt, D-64289 Darmstadt, Germany*
[5]*Institut de Recherches Subatomiques, Université Louis Pasteur, F-67037 Strasbourg, France*
[6]*Vakgroep Subatomaire en Stralingsfysica, Universiteit Gent, B-9000 Gent, Belgium*

(Received 22 November 2007; published 4 June 2008)

The (d,^{2}He) charge-exchange reaction on the double-β decay ($\beta\beta$) nucleus ^{64}Zn has been studied at an incident energy of 183 MeV. The two protons in the $^1S_0$ state (indicated as ^{2}He) were both momentum analyzed and detected simultaneously by the BBS magnetic spectrometer and its position-sensitive detector. ^{2}He spectra with a resolution of about 115 keV (FWHM) have been obtained allowing identification of many levels in the residual nucleus ^{64}Cu with high precision. ^{64}Zn is one of the rare cases undergoing a $\beta\beta$ decay in β^+ direction. In the experiment presented here, Gamow-Teller (GT$^+$) transition strengths have been extracted. Together with the GT$^-$ transition strengths from ^{64}Ni(^{3}He,t) data to the same intermediate nucleus ^{64}Cu, the nuclear matrix elements of the $\beta\beta$ decay of ^{64}Zn have been evaluated. Finally, the GT$^\pm$ distributions are compared with shell-model calculations and a critical assessment is given of the various residual interactions presently employed for the pf shell.

DOI: 10.1103/PhysRevC.77.064303 PACS number(s): 25.45.Kk, 23.40.Bw, 23.40.Hc, 27.50.+e

I. INTRODUCTION

Charge-exchange reactions of (p, n) and (n, p) type at intermediate energies and at forward angles, i.e., low momentum transfers ($q_{\rm tr} \sim 0$ and $\Delta L = 0$), selectively excite Gamow-Teller (GT) transitions because of the dominance of the $V_{\sigma\tau}$ component of the effective interaction [1–4]. However, experiments that employ the elementary (p, n) and (n, p) reactions have rather limited resolution and alternatives to them have now successfully been established through the (n, p)-type (d,^{2}He) or (t,^{3}He) reactions and the (p, n)-type (^{3}He,t) reaction. These can be performed at the Kernfysisch Versneller Instituut (KVI), Groningen [5,6], at the National Superconducting Cyclotron Laboratory at Michigan State University [7], and at the Research Center for Nuclear Physics (RCNP), Osaka [8,9]. Resolutions on the order of 100 keV in the case of (d,^{2}He), 190 keV for (t,^{3}He), and 30 keV for (^{3}He,t) can routinely be achieved. Such high-resolution charge-exchange experiments, as shown in Ref. [10,11], are of particular importance when extracting the $2\nu\beta\beta$ decay matrix element.

The nucleus ^{64}Zn presented here is an example of a system that can decay in the $\beta^+\beta^+$ direction. In this direction the electron capture (β^+EC or ECEC) process usually competes with the $\beta^+\beta^+$ decay, as the $\beta^+\beta^+$ mode requires a decay Q value in excess of $4m_ec^2 = 2.044$ MeV, which significantly reduces the available phase space. In ^{64}Zn the decay Q value is 1.096 MeV, which makes the electron capture modes, β^+ EC and ECEC, the only possible decay modes. Further, whereas in the 2νECEC mode, the two neutrinos carry away the excess decay energy, this energy must be emitted in the neutrinoless mode through a radiative process ($0\nu\gamma$ECEC) [12–14]. In the case of ^{64}Zn this amounts to a γ-ray energy of 1.096 MeV minus the atomic excitation energy of the daughter.

In the 1950s measurements on the ECEC decay of ^{64}Zn were performed by Berthelot *et al.* using x-ray detectors to detect the K-shell capture [15] and by Fremlin *et al.* using photographic emulsion plates [16]. Lower limits for the decay half-life were given as $T_{1/2}^{(\rm ECEC)} \geqslant 0.8 \times 10^{16}$ yr and $T_{1/2}^{(\rm ECEC)} \geqslant 2 \times 10^{17}$ yr, respectively. An early experiment to examine the β^+EC decay of ^{64}Zn was performed by Norman [17] at Lawrence Berkeley Laboratory using a sample of natural Zn (48.6% ^{64}Zn) sandwiched between two Ge-detectors to detect the annihilation signal of the emitted positron. A lower limit of $T_{1/2}^{(\beta^+{\rm EC})} \geqslant 2.3 \times 10^{18}$ yr was deduced. More recently, ^{64}Zn is being used in the $\beta\beta$ experiments of the COBRA collaboration [18] and the $\beta\beta$-decay project by Watanabe *et al.* [19], where the decay is studied in the CdZnTe detectors. First results from a prototype of the COBRA setup have recently been published [20], which are in accordance with previously published results from Danevich *et al.* using $ZnWO_4$ [21].

Predicted half-lives for the decays 2νECEC, $2\nu\beta^+$EC, or $2\nu\beta^+\beta^+$ (if allowed by Q value) are of the order of 10^{22-25} yr, 10^{24-26} yr, and 10^{27-30} yr, respectively, making the experimental detection difficult [22,23]. However, if there were positive

[*]Present address: PHILIPS Research Europe, 52066 Aachen, Germany.
[†]Permanent address: NIPNE, Bucharest, Romania.
[‡]Present address: EADS Astrium Space Transportation GmbH, TE53 Avionics Engineering, 28199 Bremen, Germany.

observation of the $0\nu\beta^-\beta^-$ decay mode, the 0ν decay mode in the β^+ direction could be used to distinguish between the neutrino-mass mechanism and right-handed currents [24].

The connection of the $2\nu\beta\beta$ decay rate with the nuclear matrix element is given by

$$\Gamma^{2\nu}_{(\beta^+\beta^+)} = G^{2\nu}(Q, Z)\left|M^{(2\nu)}_{\mathrm{DGT}}\right|^2, \tag{1}$$

where $G^{2\nu}(Q, Z)$ is a phase-space factor depending on the Q value of the reaction, the weak coupling constant, and the Z value of the decaying nucleus [25]. The $2\nu\beta\beta$ decay matrix element for the $\beta^+\beta^+$ direction can be deduced by combining GT^+ and GT^- distributions in the following way [26]:

$$M^{(2\nu)}_{\mathrm{DGT}} = \sum_m \frac{\langle 0^{(f)}_{\mathrm{g.s.}}||\sum_k \sigma_k\tau^+_k||1^+_m\rangle\langle 1^+_m||\sum_k \sigma_k\tau^+_k||0^{(i)}_{\mathrm{g.s.}}\rangle}{{}^1/_2 Q_{\beta\beta}\left[0^{(f)}_{\mathrm{g.s.}}\right] + E_x(1^+_m) - E_0}$$

$$= \sum_m \frac{M^{\mathrm{GT}^-}_m \times M^{\mathrm{GT}^+}_m}{{}^1/_2 Q_{\beta\beta}\left[0^{(f)}_{\mathrm{g.s.}}\right] + E_x(1^+_m) - E_0}. \tag{2}$$

Here, $E(1^+_m) - E_0$ is the energy difference between the mth intermediate 1^+ state and the initial ground state, and the sum $\sum_k$ is taken over all protons of the decaying nucleus [27,28]. Contributions from Fermi-type virtual transitions are negligible, because initial and final states belong to different isospin multiplets. The transition matrix is a sum of products of two ordinary β-decay GT matrix elements between the initial and the intermediate states and between the intermediate states and the final ground state. These matrix elements are experimentally accessible through charge-exchange reactions in the β^+ and β^- directions at intermediate energies of 100-200 MeV/nucleon [1,2,10,26,29–32] or, for the ground-state transitions, through a measurement of the single β^+/EC and β^--decay rates [33]. Figure 1 depicts the situation for the $\beta\beta$ decay of ^{64}Zn.

The study of the nucleus ^{64}Zn through (n, p)-type charge-exchange reactions has another interesting aspect for the $2\nu\beta\beta$ decay. As ^{64}Zn lies on the proton-rich side of the valley of stability (e.g., for ^{64}Zn, $N - Z = 4$), GT^+ transitions for these nuclei should be significantly less Pauli-blocked than those of their counterparts on the neutron-rich side. Relaxing the Pauli blocking can have a marked effect on the overall size of the nuclear matrix element, thereby significantly accelerating the 2ν decay.

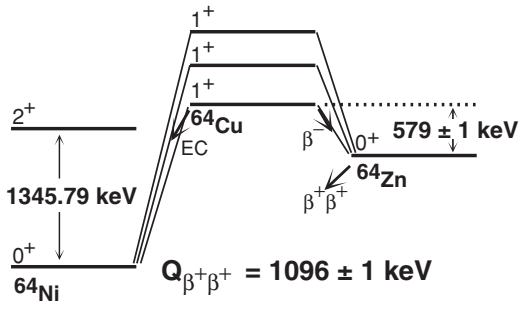

FIG. 1. Schematic representation of the $\beta\beta$ decay of ^{64}Zn. The transitions are given together with the corresponding Q values. In the final nucleus the first excited state in ^{64}Ni is at 1.346 MeV [34].

In this article, results of the ^{64}Zn$(d,{}^2\mathrm{He})^{64}$Cu experiment are presented. The experiment was performed at KVI at an incident deuteron energy of 183 MeV. The data are compared with those from the ^{64}Ni$({}^3\mathrm{He},t)^{64}$Cu experiment, which was performed at RCNP, by Popescu *et al.* [35] using a 420-MeV ^{3}He beam.

II. EXPERIMENT

The $(d,{}^2\mathrm{He})$ experiment was carried out using the ESN-BBS setup of the Accelerateur Groningen-Orsay (AGOR) facility at KVI, Groningen [36,37]. Deuterons of 183 MeV were delivered by the superconducting cyclotron AGOR. Beam line and Big-Bite magnetic spectrometer (BBS) were set up in dispersion-matched mode to ensure optimum energy resolution. The spectrometer was set to $\Theta_{\mathrm{BBS}} = 0^\circ$, 2.5°, and 5° to be able to extract angular distributions. Beam currents were measured with a Faraday cup inside the spectrometer and ranged between 0.5 and 1.5 nA. A self-supporting ^{64}Zn foil (99.7%) with a thickness of 2 mg/cm^2 was used as target. The outgoing ^{2}He were momentum analyzed by the BBS through coincident detection of the two protons in the EuroSuperNova detector (ESN detector). The ESN detector is a focal-plane detection system consisting of two vertical-drift chambers and a set of four multiwire proportional chambers acting as an additional tracking detector [38,39].

A full account of how the $(d,{}^2\mathrm{He})$ experiments are analyzed is given in Refs. [5,40,41]. In this experiment an energy resolution of about 115 keV was achieved.

III. ANALYSIS

A ^{64}Zn$(d,{}^2\mathrm{He})$ excitation-energy spectrum is shown in Fig. 2 (upper part). Known levels in ^{64}Cu were used for the energy calibration. Unfortunately, hydrogen contaminations can never be avoided and a signal of the ^{1}H$(d,{}^2\mathrm{He})n$ transition appears in the 0° spectrum at $\approx +0.2$ MeV with respect to the excitation-energy frame of ^{64}Cu. However, the hydrogen signal is well known and can be used for energy and angle calibration purposes. As a result of different kinematics, the hydrogen peak moves to higher excitation energy with increased angle and quickly broadens.

A. DWBA analysis

The J^π assignments of the excited states have been made by comparing angular distributions to distorted-wave Born approximation (DWBA) calculations. The DWBA calculations were performed using the ACCBA code of Okamura [42], which treats the $(d,{}^2\mathrm{He})$ reaction in an ordinary distorted-wave formalism and the three-body problem of the exit channel in an adiabatic approximation.

Deuteron- and proton-scattering wave functions in the entrance and exit channels are described using optical-model parameters (OMPs). Deuteron OMPs have recently been determined from a (d, d') measurement on various nuclei up to masses $A = 116$ by Korff *et al.* [43], from which

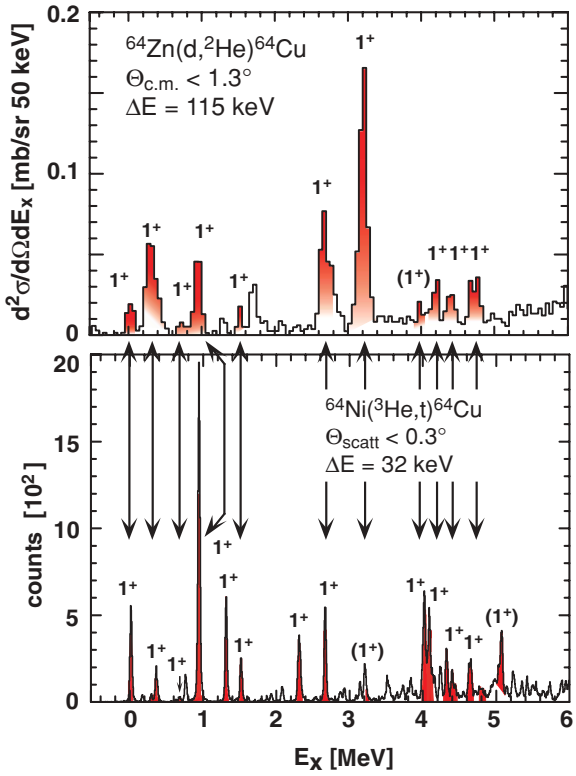

FIG. 2. (Color online) Excitation-energy spectra for ^{64}Zn $(d,^2\mathrm{He})^{64}$Cu (upper panel) and ^{64}Ni$(^3\mathrm{He},t)^{64}$Cu (lower panel, from Ref. [35]). The $(d,^2\mathrm{He})$ spectrum was taken at a spectrometer angle of 0° and covers an angular range in the center-of-mass system between 0° and 1.3°. The J^π of individual levels were determined by the shape of the cross-section angular distributions. A weak hydrogen contamination in the $(d,^2\mathrm{He})$ reaction appears around 0.2 MeV, although it is not readily visible in the spectrum.

the present parameter set for mass $A = 64$ was interpolated. The proton OMPs were taken from Ref. [44]. The reaction calculations are rather insensitive to variations of the OMPs to within reasonable bounds and tuning of any of the parameters is not required. The effective interaction was interpolated from the free NN t-matrix parametrizations of Franey and Love [45] to a projectile energy of 90 MeV/nucleon. Nuclear wave functions and one-body transition densities (OBTDs) were generated by the shell-model code NORMOD [46,47] using occupation numbers deduced from a shell model with a smeared Fermi surface.

The angular distributions of GT transitions ($0^+ \rightarrow 1^+$) can easily be distinguished from the ones leading to higher J^π states, like 2^-, 2^+, or 3^+, which usually are the most relevant ones to be taken into account. The tensor-τ component of the effective interaction is a possible source of $\Delta L = 2$ transitions to 1^+ states, which interfere with GT transitions and can amount to about 20% systematic error for weakly excited transitions. However, the angular distributions for most of the excited 1^+ transitions do not give strong indications for sizable tensor-τ contributions, as these would give rise to a flattening of the angular distribution near 0°.

Referring to Fig. 2, one can identify a number of well isolated transitions up to about 5 MeV, which is remarkable as the level density in the odd-odd nucleus ^{64}Cu is appreciable at these energies. In cases where the peaks contain several closely spaced transitions, some of them even with different J^π values, we took the approach of analyzing them together. This is the case for the structures in the energy intervals [0.2–0.6 MeV] and [2.6–2.8 MeV]. In Fig. 3 we show the results of six selected transitions: the ground-state transition, the structures in the intervals [0.2–0.6 MeV] and [2.6–2.8 MeV], the isolated transition at 3.19 MeV, and the weak transitions at 2.29 MeV and 5.06 MeV.

The angular distribution of the ground-state transition shows the characteristics of a $0^+ \rightarrow 1^+$ GT transition. The broad peak in the energy bin [0.2–0.6MeV] consists of unresolved levels, including the known 1^+ transition at 0.344 MeV [48]. At 0.73 MeV we observe a weak transition, which we correlate with the known 1^+ level at 0.66 MeV [48] that is also weakly excited in the $(^3\mathrm{He},t)$ reaction [35]. The state at 1.70 MeV is identified as a strong 2^- state and is the only 2^- state easily visible in the 0° spectrum.

At 2.29 MeV a weakly excited 2^- level is identified. The peak is barely visible in the 0° spectrum as its cross section is small at low momentum transfer but increases with scattering angle. The experimental angular distribution shown in Fig. 3 is reproduced by a DWBA calculation for a 2^- transition, although an additional small 1^+ component cannot be excluded.

The peak around 2.7±0.1 MeV is broader than, e.g., the one at 3.19 MeV and rather asymmetric. The slope of the angular distribution is less steep than expected for a 1^+ transition, which is an indication for unresolved nearby states of a different spin. The detailed analysis of the $(d,^2\mathrm{He})$ spectrum reveals two unique 1^+ states, one at 2.66 ± 0.06 MeV and another at 2.78 ± 0.06 MeV with some underlying contribution of higher spin. A combination of a 1^+ and 2^- transition in the DWBA calculation reproduces the experimental angular distribution of this peak structure as shown in Fig. 3.

The strong transition at 3.19 MeV is an isolated 1^+ transition, whose angular distribution is well reproduced by the calculation (Fig. 3). The transition at 5.06 MeV is identified as a 2^- transition (Fig. 3).

The J^π assignments of the various levels in ^{64}Cu excited through the ^{64}Zn$(d,^2\mathrm{He})$ reaction are in overall agreement with those from the recent ^{64}Ni$(^3\mathrm{He},t)$ measurements [35] except for the levels at 2.29 and 5.06 MeV [identified as (2.28+2.30)-MeV and 5.0-MeV levels through $(^3\mathrm{He},t)$]. These levels were given a 1^+ assignment in the ^{64}Ni$(^3\mathrm{He},t)$ experiment [35], yet the present analysis cannot confirm this. However, the level density around 5 MeV is high and the transitions appearing in the $(d,^2\mathrm{He})$ and $(^3\mathrm{He},t)$ spectrum could well be different. Further, the level at 4.01 MeV, which has a 0° cross section of 0.044 mb/sr, is too weak to be followed to larger angles, thereby making a J^π assignment on basis of the $(d,^2\mathrm{He})$ data unreliable. Instead, we assume the $(^3\mathrm{He},t)$ result to give a correct value, as the energy resolution of $\Delta E = 32$ keV is superior for identifying weakly excited states.

DWBA calculations have been used to extract the GT$^+$ contribution either from single transitions or from energy bins through a multipole decomposition using the distinct shape of each multipole.

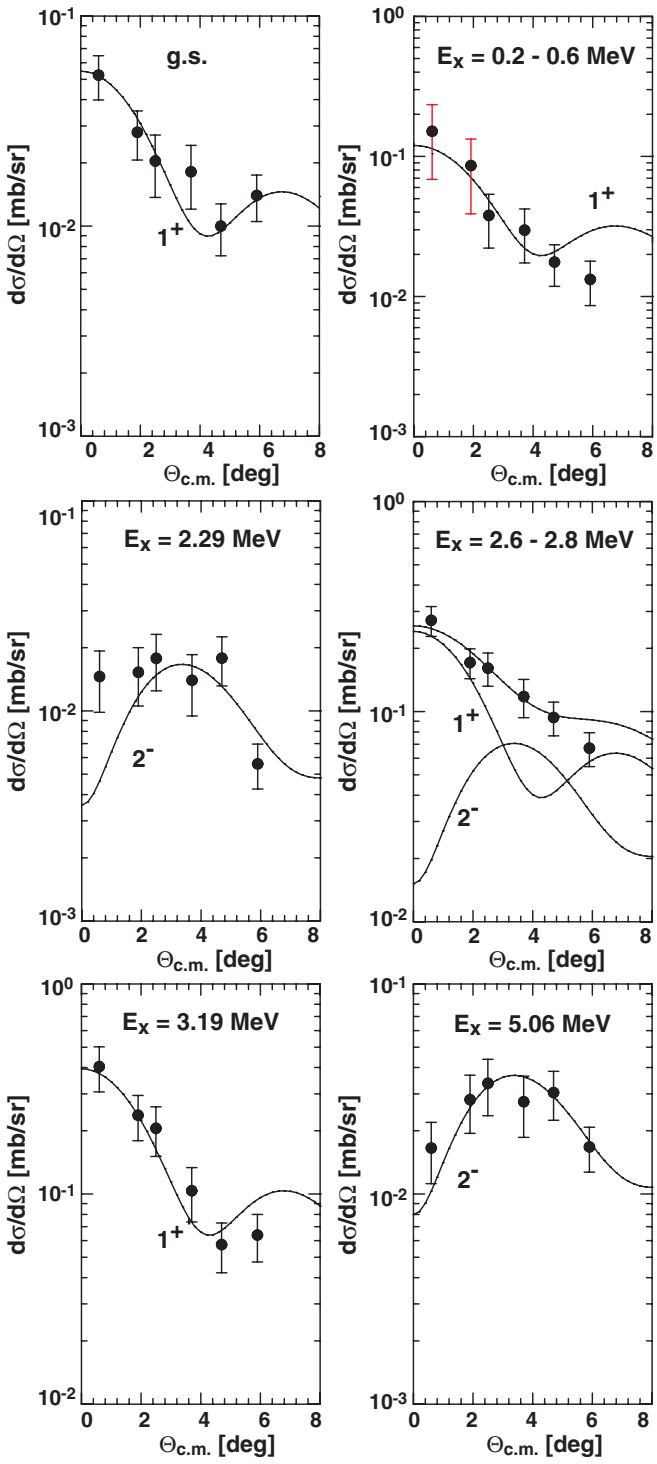

FIG. 3. (Color online) Angular distributions of the transitions discussed in the text sorted by excitation energy. DWBA calculations are represented by solid lines. The increased error bars (red) for the cross sections of the 0.2 MeV $\leqslant E_x \leqslant$ 0.6 MeV energy bin at small angles are due to the hydrogen contamination (see text). For all other data points the error bars reflect the statistical errors and an additional uncorrelated 10% systematic error due to the procedure of counting rate extraction.

B. Determination of Gamow-Teller strength

To determine the GT^+ strength, the experimental cross section $\sigma(\Theta, q_{tr})$ is first extrapolated to zero momentum transfer (i.e., $q_{tr} = 0$) by using DWBA calculations:

$$\frac{d\sigma(q_{tr}=0)}{d\Omega} = \frac{\sigma_{DWBA}(q_{tr}=0)}{\sigma_{DWBA}(\Theta, q_{tr})} \times \frac{d\sigma_{exp.}(\Theta, q_{tr})}{d\Omega}. \quad (3)$$

In the case of ^{64}Zn, the ground-state transition from ^{64}Cu has a $\log ft$ value of 5.294 $\pm$ 0.005 [34], from which the GT^+ transition strength can be evaluated through:

$$ft = \frac{(6146 \pm 6)s}{g_A^2 B(GT)}, \quad (4)$$

with $g_A = 1.2566$ [49]. By this conversion a unit cross section can be deduced to transform the cross section $\sigma(q_{tr} = 0)$ into GT^+ strength. The procedure was also applied in Ref. [35] to extract $B(GT^-)$ values from the (^{3}He,t) data using the $\log ft$ of the β^+ decay.

The extracted individual $B(GT^+)$ values below an excitation energy of 5 MeV are given in Table I. In Fig. 4, those $B(GT^+)$ values are compared to the $B(GT^-)$ values deduced from the (^{3}He,t) reaction [35]. As an additional consistency check and to assess possible contributions from weakly excited GT^+ transitions, we have further taken cross-section angular distributions of two wide excitation-energy bins, one ranging from 0 to 5 MeV and one from 5 to 10 MeV. These distributions were then analyzed performing a multipole decomposition, which included calculated $1^+, 2^-$, and 3^+ transitions. The resulting GT^+ strength in the first bin from 0 to 5 MeV is $B(GT^+) = 1.6 \pm 0.4$, which is in good agreement with the summed strength given in Table I. In the second energy

TABLE I. Table of extracted GT^+ values. The errors are statistical errors only. A systematic error of about 14% [as a result of the statistical uncertainty of the ground-state (g.s.) cross section] has to be added for all extracted values at excitation energies below 4 MeV and 20% for those above 4 MeV, the latter being a consequence of increased background due to increased level density.

E_x (MeV)	$d\sigma(q_{tr}=0)/d\Omega$ mb/sr	$B(GT^+)$
g.s.	0.056 ± 0.008	0.059 ± 0.008
0.2–0.6	0.170 ± 0.034	0.182 ± 0.034
0.73	0.022 ± 0.005	0.023 ± 0.005
0.95	0.131 ± 0.011	0.140 ± 0.012
1.52[a]	0.032 ± 0.005	0.033 ± 0.006
2.66	0.189 ± 0.015	0.193 ± 0.020
2.78	0.093 ± 0.011	0.095 ± 0.013
3.19	0.476 ± 0.020	0.512 ± 0.021
4.01[a,b]	0.044 ± 0.006	0.036 ± 0.010
4.19	0.084 ± 0.008	0.090 ± 0.008
4.39	0.081 ± 0.008	0.087 ± 0.008
4.67[a]	0.069 ± 0.007	0.067 ± 0.011
4.76	0.082 ± 0.008	0.089 ± 0.008
Σ		1.604 ± 0.054

[a]Angular distribution shows contributions from $J^\pi = 2^-$.
[b]Cross section too weak for J^π assignment (refer to text).

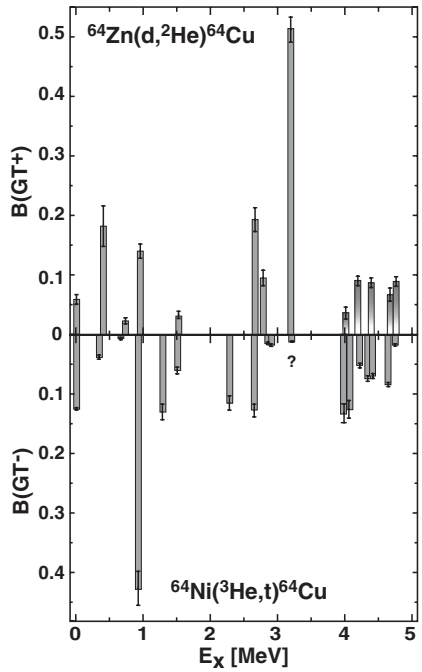

FIG. 4. Bar plot of the extracted GT$^{\pm}$ strength in ^{64}Cu from the $(d,^2\mathrm{He})$ and $(^3\mathrm{He},t)$ reactions. States above 4 MeV are dimmed to indicate uncertainties arising from the multipole decomposition. $B(\mathrm{GT}^-)$ values were taken from Ref. [35].

bin from 5 to 10 MeV, where in the zero-degree spectrum individual levels are not visible above $B(\mathrm{GT}^+) = 0.07$ units, the integrated GT$^+$ strength is analyzed to be $B(\mathrm{GT}^+) = 1.1 \pm 0.6$ units. The larger errors in both cases reflect the higher level of ambiguity of such a procedure. Further, one may also exercise caution, as for weakly excited states the tensor contributions cannot easily be estimated from such a coarse analysis [50–54]. These could turn out to be appreciable and thereby reduce the above value by a substantial fraction. A similar analysis procedure applied to excitation energies above 10 MeV turns out to be even less meaningful.

C. Consistency of the $(d, {}^2\mathrm{He})$ reaction calibration

An alternative method to determine the GT$^+$ strength was introduced by Rakers *et al.* [6]. As the $(d,^2\mathrm{He})$ cross section depends on the range of integration over the ^{2}He internal energy ε, and further, because of the likely more complicated nature of the $(d,^2\mathrm{He})$ reaction mechanism, there is an additional factor C needed to relate the measured $(d,^2\mathrm{He})$ cross-section yield to the $B(\mathrm{GT}^+)$ strength in a similar way as expressed in Ref. [2]. For a one-step process, one can assume this factor to be independent of the target mass. The relation between cross section and GT strength then is:

$$\left[\frac{d\sigma(q_{\mathrm{tr}}=0)}{d\Omega}\right]_{(d,^2\mathrm{He})} = C\left[\left(\frac{\mu}{\pi\hbar^2}\right)^2 \frac{k_f}{k_i} N_D J_{\sigma\tau}^2 B(\mathrm{GT}^+)\right]. \tag{5}$$

The parameter C was determined using $B(\mathrm{GT}^+)$ values known either from ft values or from the isospin-symmetry relation for $N = Z$ nuclei, $B(\mathrm{GT}^-) = B(\mathrm{GT}^+)$. The analysis of numerous GT transitions in the mass range $12 \leqslant A \leqslant 32$ yielded a value $C = 0.320 \pm 0.027$ [41]. This value also gave consistent results for some pf-shell nuclei like ^{48}Ti [10], ^{50}V [40], and ^{51}V [55].

Because in the present case the $B(\mathrm{GT}^+)$ value is known from the $\log ft$, one can as well use Eq. (5) to determine the factor C. In doing so, the distortion factor N_D is computed (using the ACCBA code) by the ratio of the distorted-wave (DW) to plane-wave (PW) cross sections (see Ref. [41])

$$N_D = \frac{\sigma_{\mathrm{DW}}(q_{\mathrm{tr}}=0)}{\sigma_{\mathrm{PW}}(q_{\mathrm{tr}}=0)}, \tag{6}$$

which gives a value of $N_D = 0.051$ for the ^{64}Zn$(d,^2\mathrm{He})^{64}$Cu reaction. The volume integral of the effective central $V_{\sigma\tau}$ interaction is taken as $|J_{\sigma\tau}| = 165$ MeV fm^3 [56]. Following this, C is evaluated to be $C = 0.305 \pm 0.043$, which agrees remarkably well with the value from Ref. [41] and indicates that at least up to mass $A \sim 60$ there is little mass dependence.

IV. APPLICATION TO DOUBLE-β DECAY

In Fig. 5 (top) we show the cumulative sum of the GT$^+$ strength from the present ^{64}Zn$(d,^2\mathrm{He})$ experiment. The total integrated GT$^+$ strength from the individual levels up to 5 MeV amounts to $\sum B(\mathrm{GT}^+) = 1.60 \pm 0.05(\mathrm{stat}) \pm 0.25(\mathrm{sys})$. Beyond 5 MeV we do not see any further strong states, although

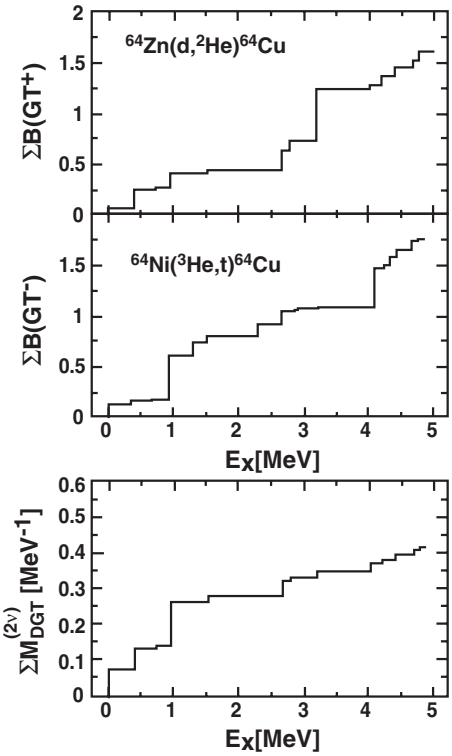

FIG. 5. Running sum of the GT$^+$ (top) and GT$^-$ strength (middle) deduced in $(d,^2\mathrm{He})$ and $(^3\mathrm{He},t)$ reactions, respectively. $(^3\mathrm{He},t)$ data are taken from Ref. [35]. The cumulative sum of the $M_{\mathrm{DGT}}^{(2\nu)}$ is shown in the lower plot.

the general background due to the high level density is not excessive and would allow detection of single states with $B(\mathrm{GT}^+)$ values greater than 0.07 units. The cumulative sum of the GT^- strength deduced from the ^{64}Ni(^{3}He,t) experiment [35] is given in the middle part of Fig. 5. Its total integrated strength amounts to $\sum B(\mathrm{GT}^-) = 1.73 \pm 0.05(\mathrm{stat}) \pm 0.2(\mathrm{sys})$. Remarkably, the above quoted GT^+ strength is of the same size. Certainly, the reduced Pauli blocking due to the low neutron excess in ^{64}Zn has a role in this.

From the individual $B(\mathrm{GT})$ values single GT matrix elements $M(\mathrm{GT})$ have been calculated and connected to the cumulative double Gamow-Teller matrix element $M_{\mathrm{DGT}}^{(2\nu)}$ according to Eq. (2). However, the one-to-one matching of levels from the two different reaction directions becomes less certain for levels above 4 MeV and the results given in Table II represent a best-try effort. One could use an alternative approach by first adding the $B(\mathrm{GT}^+)$ and $B(\mathrm{GT}^-)$ values individually in the energy interval between 4 and 5 MeV and then joining them to a combined total matrix element using an average excitation energy. This constitutes closure approximation for a limited excitation-energy window [27,57]. The resulting matrix element in the first case is $\sum_{(4-5\ \mathrm{MeV})} M_{\mathrm{DGT}}^{(2\nu)} = 0.07 \pm 0.02\ \mathrm{MeV}^{-1}$ and in the second case $M_{\mathrm{DGT}}^{(2\nu)}(4-5\ \mathrm{MeV}) = 0.09 \pm 0.03\ \mathrm{MeV}^{-1}$, which indicates a reasonably high level of consistency.

The cumulative sum of the double Gamow-Teller matrix element $M_{\mathrm{DGT}}^{(2\nu)}$ taken from Table II is shown in the lower part of Fig. 5. We note that all individual $M_{\mathrm{DGT}}^{(2\nu)}$ matrix elements were added constructively to a total value of (errors added in quadrature):

$$\sum_{E_x \leqslant 5\ \mathrm{MeV}} M_{\mathrm{DGT}}^{(2\nu)} = 0.41 \pm 0.04\ \mathrm{MeV}^{-1}.$$

Using the phase-space factors for $2\nu\beta^+\mathrm{EC}$ and $2\nu\mathrm{ECEC}$ decay given in Ref. [58] one then arrives at half-lives for the ^{64}Zn decay:

$$T_{1/2}(2\nu\beta^+\mathrm{EC}) = (4.7 \pm 0.9) \times 10^{31}\ \mathrm{yr}$$
$$T_{1/2}(2\nu\mathrm{ECEC}) = (1.2 \pm 0.2) \times 10^{25}\ \mathrm{yr}.$$

The size of the nuclear matrix element deserves to be commented on. In Refs. [10,11] a similar analysis was performed for the $\beta^-\beta^-$ decay nucleus ^{48}Ca and in Ref. [29] for ^{116}Cd. In both cases the nuclear matrix elements for the $2\nu\beta\beta$ decay were about one order of magnitude smaller (consistent with the matrix element deduced from the half-lives). The larger matrix element of ^{64}Zn could thereby accelerate the $2\nu\beta\beta$ decay by about 2 orders of magnitude, which indicates the general importance of the nuclear structure that enters into the dynamics of the $\beta\beta$ decay (see also footnote[1]). Unfortunately,

[1]One may note that the shell-model calculations quoted in Sec. V predict a reduction of the double β-decay matrix element due to phase cancellations by a factor of 0.4 and 0.7 depending on the interaction.

TABLE II. Table of all extracted $B(\mathrm{GT}^\pm)$ and $M(\mathrm{GT}^\pm)$ values and the individual $\beta\beta$ decay matrix elements $M_{\mathrm{DGT}}^{(2\nu)}$. The errors are statistical errors only. For $B(\mathrm{GT}^+)$ values a systematic error of about 14% has to be added for all extracted values at excitation energies below 4 MeV and 20% for those above, whereas for the $B(\mathrm{GT}^-)$ values a 10% systematic error was assumed ($B(\mathrm{GT}^-)$ values taken from Ref. [35]). For the summed values the combined statistical and systematic errors are quoted separately.

$E_x(d,^2\mathrm{He})$ (MeV)	$B(\mathrm{GT}^+)$	$M(\mathrm{GT}^+)$	$E_x(^3\mathrm{He},t)$ (MeV)	$B(\mathrm{GT}^-)$	$M(\mathrm{GT}^-)$	$M_{\mathrm{DGT}}^{(2\nu)}$ (MeV^{-1})
g.s.	0.059 ± 0.008	0.24 ± 0.02	g.s.	0.123 ± 0.002	0.35 ± 0.01	0.076 ± 0.011
0.2–0.6	0.182 ± 0.034	0.43 ± 0.04	0.34	0.037 ± 0.003	0.19 ± 0.01	0.056 ± 0.012
0.73	0.023 ± 0.005	0.15 ± 0.02	0.66	0.006 ± 0.001	0.08 ± 0.01	0.007 ± 0.002
0.95	0.140 ± 0.012	0.37 ± 0.02	0.92	0.426 ± 0.033	0.65 ± 0.03	0.119 ± 0.014
			1.30	0.129 ± 0.010	0.36 ± 0.01	
1.52	0.033 ± 0.006	0.18 ± 0.02	1.50	0.059 ± 0.005	0.24 ± 0.01	0.017 ± 0.003
			2.28 / 2.30	0.114 ± 0.009	0.34 ± 0.03	
2.66	0.193 ± 0.020	0.44 ± 0.03	2.64	0.125 ± 0.010	0.35 ± 0.01	0.041 ± 0.006
2.78	0.095 ± 0.013	0.31 ± 0.02	2.85	0.014 ± 0.001	0.12 ± 0.01	0.009 ± 0.001
			2.90	0.017 ± 0.001	0.13 ± 0.01	
3.19	0.512 ± 0.021	0.72 ± 0.02	3.21[a]	0.011 ± 0.001	0.10 ± 0.01	0.017 ± 0.003
4.01[a]	0.036 ± 0.010	0.19 ± 0.03	4.07	0.373 ± 0.029	0.61 ± 0.02	0.022 ± 0.006
4.19	0.090 ± 0.008	0.30 ± 0.01	4.22	0.054 ± 0.004	0.23 ± 0.01	0.013 ± 0.002
			4.31	0.077 ± 0.006	0.28 ± 0.01	
4.39	0.087 ± 0.008	0.30 ± 0.01	4.41	0.065 ± 0.005	0.26 ± 0.01	0.014 ± 0.002
4.67[b]	0.067 ± 0.011	0.26 ± 0.02	4.64	0.085 ± 0.007	0.29 ± 0.01	0.013 ± 0.002
4.76	0.089 ± 0.008	0.30 ± 0.01	4.74	0.016 ± 0.001	0.13 ± 0.01	0.006 ± 0.001
Σ	$1.604^{\pm 0.05(\mathrm{stat})}_{\pm 0.25(\mathrm{sys})}$	$4.19^{\pm 0.08(\mathrm{stat})}_{\pm 0.33(\mathrm{sys})}$		$1.730^{\pm 0.05(\mathrm{stat})}_{\pm 0.17(\mathrm{sys})}$	$4.71^{\pm 0.05(\mathrm{stat})}_{\pm 0.23(\mathrm{sys})}$	$0.41^{\pm 0.02(\mathrm{stat})}_{\pm 0.04(\mathrm{sys})}$

[a]Cross section too weak for J^π assignment.
[b]$J^\pi = 2^-$ contributions of about 10%.

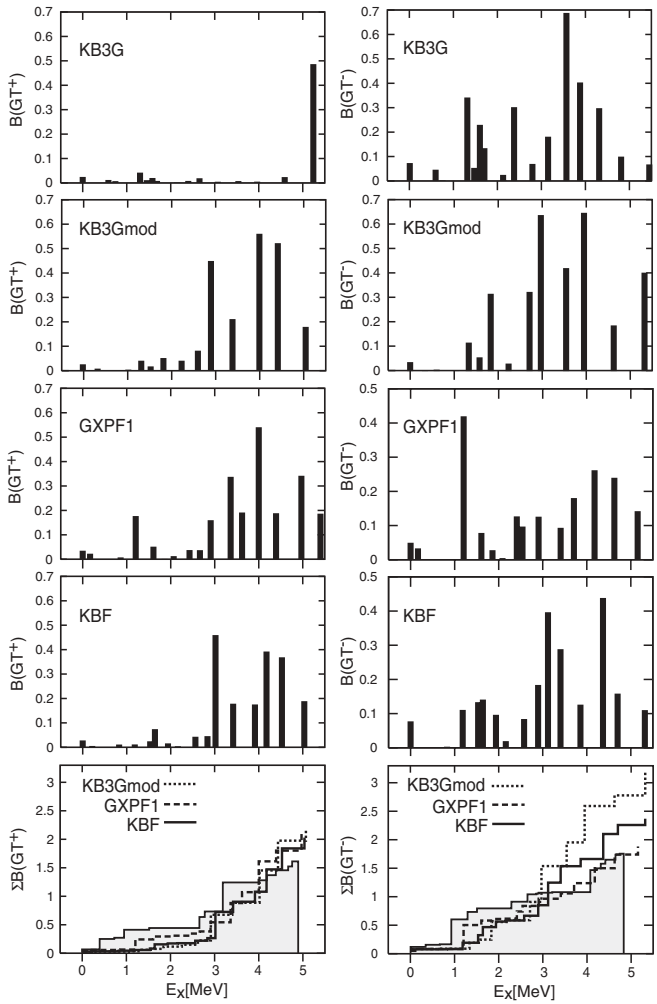

FIG. 6. GT^+ and GT^- strength distributions and their running sums for the daughter nucleus ^{64}Cu at low excitation energies calculated with KB3G, its gap-corrected version KB3Gmod, GXPF1, and KBF effective interactions. The shaded area represents the experimental curve.

this rather advantageous factor does not offset the large extra suppression, which enters through the $\beta^+\beta^+$ phase-space factor compared to the $\beta^-\beta^-$ case, let alone the experimental difficulties associated with the detection of the decay. This large phase-space suppression is, in fact, a general feature of nearly all nuclei, which decay in the $\beta^+\beta^+$ direction.

V. COMPARISON WITH THEORETICAL SHELL-MODEL CALCULATIONS

Apart from properties of the $\beta\beta$ decay, GT^+ and GT^- strength distributions are as well important in many astrophysical processes [59], as they determine the electron-capture and β^--decay rates on nuclei, and thereby the dynamics of the core collapse in a type II supernova [60,61]. For the calculation of these rates, the shell model has been identified as the model of choice for nuclei in the iron mass range [62,63]. However, the residual interaction in the pf shell is not yet sufficiently well determined, and especially for nuclei with valence nucleons above the $N = 28$ shell closure, the predictive power of shell-model calculations has not yet reached the same level of accuracy as the one for the nuclei in the lower part of the pf shell. The present detailed GT strength distributions on ^{64}Zn and ^{64}Ni provide valuable experimental input for testing various residual pf-shell interactions.

Therefore, calculations were performed with the code NATHAN [64,65] within the full pf shell. These allowed promotion of seven nucleons from the $f_{7/2}$ orbital into the rest of the shell. This truncation ensures convergence for the total GT strength and its distribution. The calculated $B(\mathrm{GT})$ values were then scaled by a constant factor of $(0.74)^2$ to account for the quenching of the measured GT strength [66]. The GT distributions were determined using the Lanczos method with 100 iterations [65]. Three different residual interactions were employed, the KBF, the KB3G, and the GXPF1 interactions. The KBF interaction [62,63] has been successful in evaluating weak interaction rates of pf-shell nuclei [63], which are currently being used in core-collapse supernova simulations [67]. It generally reproduces the measured GT strength distributions [62,68] but shows deficiencies in describing the nuclear structure around the doubly magic ^{56}Ni. Some improvements were achieved by small monopole corrections and modifications of matrix elements, which then has led to the KB3G interaction [69]. Otsuka *et al.* [70] determined the residual interaction GXPF1 by fitting the interaction matrix elements to a large selection of excitation-energy and transition data in the pf shell. A modified version of this interaction (i.e., GXPF1A) has recently been presented to describe the 2^+ excitation energy in ^{56}Ti [71].

The resulting GT strength distributions for the various interactions are shown in Fig. 6. Although not perfect in detail, the GT^+ distributions obtained with the KBF and GXPF1 interactions give a fair account of the experimental strength up to about $E_x = 4$ MeV. However, both interactions predict appreciable GT^+ strength for $E_x > 4$ MeV, which is not readily observed experimentally, and a slightly larger total GT^+ strength up to 5 MeV, $\sum B(\mathrm{GT}^+) = 2.0$(KBF), 2.1(GXPF1) (Fig. 6). The GXPF1 interaction generates additional GT^+ strength of about 0.9 units at $E_x > 5$ MeV, whereas the KBF interaction places only 0.45 units into this region. These numbers are consistent with the one extracted from the rather coarse analysis presented in Sec. III B for this energy region. Remarkably, the third residual interaction, KB3G, fails badly. It generates only little strength below 5 MeV, and most of the calculated GT^+ strength (about 1.5 units) is found in two strong transitions just above 5 MeV. This deficiency is traced back to the $Z = 28$ proton gap that seems overestimated by KB3G. After correcting this by a monopole shift of the $T = 0$ matrix elements, the total $B(\mathrm{GT}^+)$ strength remains unchanged, however, the strength is moved to lower excitation energies, in better agreement with the data (see Fig. 6, second panel).

The experimental GT^- strength is best reproduced by the GXPF1 interaction (Fig. 6, right). It reproduces the single strong transition to a state around 1 MeV, gives a fair account of the GT^- distribution for energies below 5 MeV and also reproduces the total strength in this energy interval [$\sum B(\mathrm{GT}^-) = 1.7$]. With the KBF interaction the GT^- strength in the energy interval $E_x = 1$–2 MeV is

distributed over several states. Furthermore, this interaction predicts more strength for the interval $E_x = 3$–5 MeV than is observed (about 2.4 units). However, the gap-corrected version of the KB3G interaction (i.e., KB3Gmod) generates significantly more GT^- strength below 5 MeV. Of course, only a small portion of the GT^- strength resides at $E_x <$ 5 MeV, whereas most of the strength is concentrated in the GT^- resonance, which all three interactions place above 10 MeV.

VI. CONCLUSIONS

We have demonstrated that the $(d,^2\mathrm{He})$ and the $(^3\mathrm{He},t)$ charge-exchange reactions are powerful alternatives to the elementary (n,p) and (p,n) reactions, as they provide the high resolution needed to unravel the nuclear structure that enters into the dynamics of $\beta\beta$ decay. ^{64}Zn was presented as a case study. It marks the first time that experimental $\beta\beta$-decay nuclear matrix elements have been determined for a nucleus, which can decay in the $\beta^+\beta^+$ direction. As $\beta^+\beta^+$-decaying nuclei feature a comparatively low neutron excess (e.g., $N - Z = 4$ for ^{64}Zn), the suppression owing to the Pauli blocking of occupied levels in the daughter nucleus should be significantly less severe. This is what is observed by the relatively large $B(GT^+)$ strength appearing in the ^{64}Cu daughter at low excitation energies. Likewise, the large $B(GT^+)$ values ensure a large $\beta\beta$-decay matrix element, which in the present case is about an order of magnitude larger than that of the previously investigated nuclei ^{48}Ca or ^{116}Cd.

From the theory side, the present $GT^\pm$ strength distributions for ^{64}Zn and ^{64}Ni are important benchmarks for extending the presently existing residual interactions towards the heavy nuclei in the pf shell. Although the GXPF1 and KBF interactions give acceptable results when confronted with the data, the KB3G interaction clearly did not. After reducing the proton gap in the modified version KB3Gmod the agreement with the experimental data is improved.

ACKNOWLEDGMENTS

This work was supported by the European Commission within the Sixth Framework Programme through I3-EURONS (contract no. RII3-CT-2004-506065). One of the authors, D.S., was supported by the DFG (SFB 634).

[1] C. D. Goodman *et al.*, Phys. Rev. Lett. **44**, 1755 (1980).
[2] T. N. Taddeucci *et al.*, Nucl. Phys. **A469**, 125 (1987).
[3] W. P. Alford and K. P. Jackson eds., Proc. of the Workshop on Isovector Excitations in Nuclei, Can. J. Phys. **65**, (1987).
[4] K. P. Jackson *et al.*, Phys. Lett. **B201**, 25 (1988).
[5] S. Rakers *et al.*, Nucl. Instrum. Methods B **481**, 253 (2002).
[6] S. Rakers *et al.*, Phys. Rev. C **65**, 044323 (2002).
[7] G. W. Hitt *et al.*, Nucl. Instrum. Methods A **566**, 264 (2006).
[8] T. Adachi *et al.*, Phys. Rev. C **73**, 024311 (2006).
[9] Y. Fujita *et al.*, Phys. Rev. Lett. **95**, 212501 (2005).
[10] S. Rakers *et al.*, Phys. Rev. C **70**, 054302 (2004).
[11] E.-W. Grewe *et al.*, Phys. Rev. C **76**, 054307 (2007).
[12] Z. Sujkowski and S. Wycech, Acta Phys. Pol. B **33**, 471 (2002).
[13] S. Wycech and Z. Sujkowski, Acta Phys. Pol. B **35**, 1223 (2004), nucl-th/0402103.
[14] Z. Sujkowski and S. Wycech, Phys. Rev. C **70**, 052501(R) (2004).
[15] A. Berthelot, R. Chaminade, C. Levi, and L. Papineau, présentée par M. F. Joliot, Comptes Rendus de l'Academie de Sciences, **236**, 1769 (1953).
[16] J. H. Fremlin and M. C. Walters, Proc. Phys. Soc. London A **65**, 911 (1952).
[17] E. B. Norman, Phys. Rev. C **31**, 1937 (1985).
[18] J. R. Wilson, Czech. J. Phys. **56**, 543 (2006).
[19] T. Watanabe *et al.*, Nucl. Instrum. Methods A **436**, 155 (1999).
[20] T. Bloxham *et al.*, Phys. Rev. C **76**, 025501 (2007).
[21] F. A. Danevich *et al.*, Nucl. Instrum. Methods A **544**, 553 (2005) and arXiv:nucl-ex/04090112v1 (2004).
[22] K. Zuber, Phys. Rep. **305**, 295 (1998).
[23] C. W. Kim and K. Kubodera, Phys. Rev. D **27**, 2765 (1983).
[24] M. Hirsch *et al.*, Z. Phys. A **347**, 151 (1994).
[25] J. Suhonen and O. Civitarese, Phys. Rep. **300**, 123 (1998).
[26] W. P. Alford *et al.*, Nucl. Phys. **A514**, 49 (1990).
[27] W. C. Haxton and G. J. Stephenson Jr., Prog. Part. Nucl. Phys. **12**, 409 (1984).
[28] M. Doi, T. Kotani, and E. Takasugi, Prog. Theor. Phys. Suppl. **83**, 1 (1985).
[29] S. Rakers *et al.*, Phys. Rev. C **71**, 054313 (2005).
[30] H. Ejiri, Phys. Rep. **338**, 265 (2000); J. Phys. Soc. Jpn. **74**, 2101 (2005).
[31] W. P. Alford and B. Spicer, Adv. Nucl. Phys. **24**, 1 (1998).
[32] B. D. Anderson *et al.*, Phys. Rev. C **31**, 1161 (1985).
[33] D. Frekers, J. Dilling, and I. Tanihata, Can. J. Phys. **85**, 57 (2007).
[34] R. Firestone and V. S. Shirley, *Table of Isotopes*, 8th ed. (John Wiley & Sons, Inc., New York, 1996).
[35] L. Popescu, Ph.D. thesis, Gent University (2006); L. Popescu *et al.*, to be published (2008).
[36] A. M. van den Berg *et al.*, Nucl. Instrum. Methods B **99**, 637 (1995).
[37] H. J. Wörtche *et al.*, Nucl. Phys. **A687**, 321c (2001).
[38] M. Hagemann *et al.*, Nucl. Instrum. Methods A **437**, 459 (1999).
[39] V. M. Hannen *et al.*, Nucl. Instrum. Methods A **500**, 68 (2003).
[40] C. Bäumer *et al.*, Phys. Rev. C **71**, 024603 (2005).
[41] E.-W. Grewe *et al.*, Phys. Rev. C **69**, 064325 (2004).
[42] H. Okamura, Phys. Rev. C **60**, 064602 (1999).
[43] A. Korff *et al.*, Phys. Rev. C **70**, 067601 (2004).
[44] A. J. Koning and J. P. Delaroche, Nucl. Phys. **A713**, 231 (2003).
[45] M. A. Franey and W. G. Love, Phys. Rev. C **31**, 488 (1985).
[46] A. Bohr and B. R. Mottelson, *Nuclear Structure* (Benjamin, New York, 1975), Vols. 1 and 2.
[47] M. A. Hofstee *et al.*, Nucl. Phys. **A588**, 729 (1995); S. Y. van der Werf, computer code NORMOD, KVI Groningen, 1991 (unpublished).
[48] B. Singh, Nucl. Data Sheets **108**, 197 (2007).
[49] I. S. Towner and J. C. Hardy, nucl-th/9504015 (1995).

[50] R. T. G. Zegers *et al*., Phys. Rev. C **74**, 024309 (2006).
[51] A. L. Cole *et al*., Phys. Rev. C **74**, 034333 (2006).
[52] Y. Fujita *et al*., Phys. Rev. C **75**, 057305 (2007).
[53] R. T. G. Zegers *et al*., Phys. Rev. C **77**, 024307 (2008).
[54] K. Amos, A. Faessler, and V. Rodin, Phys. Rev. C **76**, 014604 (2007).
[55] C. Bäumer *et al*., Phys. Rev. C **68**, 031303(R) (2003).
[56] W. G. Love and M. A. Franey, Phys. Rev. C **24**, 1073 (1981).
[57] J. D. Vergados, Phys. Rev. C **13**, 865 (1976).
[58] C. W. Kim and K. Kubodera, Phys. Rev. D **27**, 2765 (1983).
[59] K. Langanke and G. Martínez-Pinedo, Rev. Mod. Phys. **75**, 819 (2003).
[60] W. R. Hix *et al*., Phys. Rev. Lett. **91**, 201102 (2003).
[61] K. Langanke *et al*., Phys. Rev. Lett. **90**, 241102 (2003).
[62] E. Caurier *et al*., Nucl. Phys. **A653**, 439 (1999).
[63] K. Langanke and G. Martínez-Pinedo, Nucl. Phys. **A673**, 481 (2000).
[64] E. Caurier, G. Martinez-Pinedo, F. Nowacki, A. Poves, J. Retamosa, and A. P. Zuker, Phys. Rev. C **59**, 2033 (1999).
[65] E. Caurier *et al*., Rev. Mod. Phys. **77**, 427 (2005).
[66] G. Martínez-Pinedo, A. Poves, E. Caurier, and A. P. Zuker, Phys. Rev. C **53**, R2602 (1996).
[67] H.-T. Janka *et al*., Phys. Rep. **442**, 38 (2007).
[68] D. Frekers, Prog. Part. Nucl. Phys. **57**, 217 (2006).
[69] A. Poves *et al*., Nucl. Phys. **A694**, 157 (2001).
[70] M. Honma, T. Otsuka, B. A. Brown, and T. Mizusaki, Phys. Rev. C **65**, 061301(R) (2002).
[71] M. Honma *et al*., Eur. Phys. J. A **25**, Suppl. 1, 499 (2005).